Ferroelectrics

ISSN: 0015-0193 (Print) 1563-5112 (Online) Journal homepage: https://www.tandfonline.com/loi/gfer20

Electrical response in poled $(Bi_{0.5}Na_{0.5})_{0.935}Ba_{0.065}TiO_3$ ceramics

Nayda Patricia Arias Duque, Oscar Hernan Giraldo Osorio, Ernesto Suaste Gómez, Blanca Estela González Sanchez, Carlos O. González-Moran, Jose G. Miranda Hernández & Jose de Jesus Agustin Flores-Cuautle

To cite this article: Nayda Patricia Arias Duque, Oscar Hernan Giraldo Osorio, Ernesto Suaste Gómez, Blanca Estela González Sanchez, Carlos O. González-Moran, Jose G. Miranda Hernández & Jose de Jesus Agustin Flores-Cuautle (2020) Electrical response in poled $(Bi_{0.5}Na_{0.5})_{0.935}Ba_{0.065}TiO_3$ ceramics, Ferroelectrics, 558:1, 67-78

To link to this article: https://doi.org/10.1080/00150193.2020.1738183

Published online: 04 May 2020.

FERROELECTRICS
2020, VOL. 558, 67–78
https://doi.org/10.1080/00150193.2020.1738183

Taylor & Francis
Taylor & Francis Group

Electrical response in poled $(Bi_{0.5}Na_{0.5})_{0.935}Ba_{0.065}TiO_3$ ceramics

Nayda Patricia Arias Duque[a,b], Oscar Hernan Giraldo Osorio[b,c,d], Ernesto Suaste Gómez[e], Blanca Estela González Sanchez[f], Carlos O. González-Moran[g], Jose G. Miranda Hernández[g], and Jose de Jesus Agustin Flores-Cuautle[h]

[a]Facultad de Ciencias e Ingeniería, Grupo de Investigación Núcleo, Universidad de Boyacá, Tunja, Colombia; [b]Grupo de Investigación en Procesos Químicos, Catalíticos y Biotecnológicos, Universidad Nacional de Colombia, Sede Manizales, Colombia; [c]Departamento de Física y Química, Facultad de Ciencias Exactas y Naturales, Universidad Nacional de Colombia, Sede Manizales, Colombia; [d]Laboratorio de Materiales Nanoestructurados y Funcionales, Facultad de Ciencias Exactas y Naturales, Universidad Nacional de Colombia, Sede Manizales, Colombia; [e]Departamento de Ingeniería Eléctrica, CINVESTAV-IPN, Ciudad de México, México; [f]Tecnológico Nacional de México/I.T. Orizaba, Orizaba, Mexico; [g]Laboratorio de Investigación de Materiales y Procesos Inteligentes, Centro Universitario UAEM Valle de México; [h]CONACYT-Tecnológico Nacional de México/I.T. Orizaba, Orizaba, Mexico

ABSTRACT

A ferroelectric material $(Bi_{0.5}Na_{0.5})_{0.935}Ba_{0.065}TiO_3$ (BNBT) with a perovskite structure was poled and characterized by electrical impedance spectroscopy as a function of temperature, X-ray diffraction, and Rietveld refinement. The ac conductivity showed a low-frequency dispersion, supporting the idea of heterogeneous potential wells favored by Bi^{3+}, Na^{+}, and Ba^{2+} on the A site of the perovskite type of structure. The activation energies for ac conduction depende on the studied frequency. The permittivity and electrical modulus showed a distribution of the relaxation time associated with the delay in the orientation of the dipoles and an important contribution to the short-range conductivity.

ARTICLE HISTORY
Received 17 May 2019
Accepted 21 February 2020

KEYWORDS
Phase change; BNBT; electrical behavior; dielectric permittivity; Rietveld refinement

1. Introduction

Ferroelectric ceramics are of scientific interest due to their numerous applications, such as use as dielectric capacitors, infrared (IR) sensors, piezosensors, actuators, electrooptic shutters, and nonvolatile memory devices [1]. Among ferroelectric materials already available, lead-free ferroelectric ceramics are especially attractive due to their environmentally friendly sintering process, and they are non-hazardous in human-related applications [2, 3].

In the search for ferroelectric materials with specific properties, several lead-free ceramics have been used and different doping systems have already been developed. $Na_{0.5}Bi_{0.5}TiO_3$ is a lead-free ferroelectric that has served as a base for extensively developing piezoelectric ceramics [4, 5]. Among doping ions, divalent cations, such as Mg^{2+} [6], Ca^{2+} [7], Sr^{2+} [8], and Ba^{2+} [9], transition metals ions, such as Mn^{2+}[10], Fe^{2+}[11], Co^{2+} [12], Ni^{2+} [13], Zn^{2+}[14], Nb^{5+} [15], and W^{6+} [16], also, rare earth

CONTACT Jose de Jesus Agustin Flores-Cuautle jflores_cuautle@hotmail.com

cations, such as Ce^{3+} [17, 18], Gd^{3+} [19], Nd^{3+} [20], and Er^{3+} [21] have been used to depress the formation of charge defects [16] or to modify dielectrics and thermophysical properties.

Bismuth sodium barium titanate (BNBT) with a perovskite structure is a ferroelectric material based on barium titanate ($BaTiO_3$), which is widely known [5] for its large piezoelectric response, which is comparable to those with lead-containing $Pb(Zr,Ti)O_3$ (PZT) solid solutions [22]. There have been different compositions reported for BNBT piezoceramics, with a Ba quantity ranging from 0.05 to 0.08 molar ratio [23–31]. In particular, the pyroelectric coefficient and thermophysical properties have been studied for unpoled $(Bi_{0.5}Na_{0.5})_{0.935}Ba_{0.065}TiO_3$ (BNBT 0.935/0.065) [24, 25, 32]. For unpoled BNBT 0.935/0.065, 425 °C has been reported as the Curie temperature [32, 33] and dielectric constant around 17000 [25, 33]. In the literature there are studies on the electrical behavior of (0.67-x) $BiFeO_3$-0.33$BaTiO_{3-x}SrZrO_3$ [34] $La(Ti_{0.5}Mg_{0.5})O_3$-doped $(Bi_{0.5}Na_{0.5})TiO_3$-$(Sr_{0.7}Bi_{0.2})TiO_3$ [35], $Bi_{0.5}Na_{0.5}Ti_{1-x}Mn_xO_{3-\delta}$ [36], $Ba(Zr_xTi_{1-x})O_3$ [37], (1-x)[0.82$Bi_{0.5}Na_{0.5}TiO_3$–0.18$Bi_{0.5}K_{0.5}TiO_3$]–x$BiFeO_3$ [38] ceramics, but there is limited systematic information regarding the structure-electrical behavior for poled $(Bi_{0.5}Na_{0.5})_{0.935}Ba_{0.065}TiO_3$. In this work, the electrical response of poled BNBT (0.935/0.065) between room temperature and 300 °C was studied, with special attention to the effect of structural parameters in the conduction processes.

2. Methods

2.1. Ceramic preparation

A solid-state reaction method was used to prepare BNBT (0.935/0.065) ceramics with Bi_2O_3, TiO_2, Na_2CO_3, and $BaCO_3$ (99%+ purity, Sigma-Aldrich) as starting chemicals, which were weighed in the appropriate ratio to reach the stoichiometric formula of $(Bi_{0.5}Na_{0.5})_{0.935}Ba_{0.065}TiO_3$ based on previously works [24, 25, 32, 33]. The raw chemicals were mixed with a planetary electronic agate mill with polyvinyl alcohol (PVA) as a binder. The mixture was then calcinated at 800 °C for one h. The calcinated powder was milled again to reduce the particle size. Pellets of 10 mm diameter were formed using PVA as a binder and applying 3500 Kg/cm^2 of pressure. Pellets were sintering in an air atmosphere at 1200 °C for two h. Silver electrodes were then applied and fired at 200 °C for one h. Then, an electrical field was applied for poling the ceramics, using an oil silicone bath with a dc field of 3 kV/mm at 90 °C for one h. The sample was labeled as BNBT(0.935/0.065).

2.2. Electric measurements

The sample was placed between two platinum electrodes with a 10 mm effective diameter in a two-point configuration, and it was adjusted with a spring. A tube furnace (Thermo Scientific Lindberg F21135 Multi-Position Tube Furnace) was used to control the sample temperature. Samples were measured from room temperature up to 300 °C with steps of 25 °C. Before each measurement, 20 min periods were used as temperature stabilization times. Frequencies from 10 MHz to 0.1 Hz were used with a signal

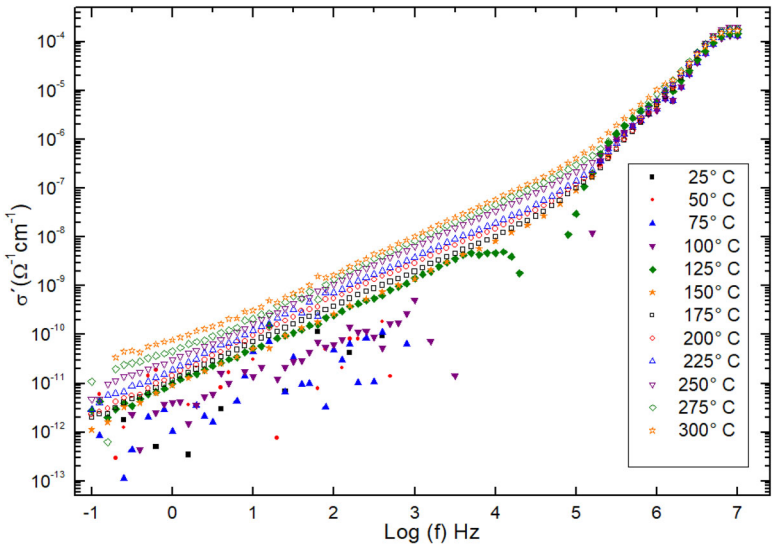

Figure 1. The real component of the complex conductivity for poled Bismuth sodium barium titanate (BNBT (0.935/0.065)).

amplitude of 100 mV RMS and 0 DC bias in a SOLARTRON 1260 Frequency Response Analyzer [39] coupled with a SOLARTRON 1296 dielectric interphase.

2.3. Structural characterization and rietveld refinement

The X-ray diffraction pattern for structural characterization was recorded from the dry ceramic bulk in a Siemens D5000 X-ray diffractometer. Cu-Kα1 radiation was used with $\lambda = 1.5406$ Å between 10° and 90° 2θ degrees, a 0.02° step size, and 0.02°/sec. These acquisition parameters have been used for perovskite materials [40, 41], and they were selected due to it is known that this perovskite type of material has high crystallinity. Therefore, the intensity of the diffraction pattern at high angles is good enough to perform the analysis [42]. The crystallographic parameters were obtained by Rietveld refinement trough GSAS-EXPGUI® software [43, 44]. For the background refinement, the shifted Chebyshev equation with eight terms was used. The Pseudo–Voigt equation was selected for profile shape function, and 32 refinement parameters were used. Vesta software ® [45] was used to draw the BNBT polyhedral structure.

3. Results and discussion

3.1. Electrical behavior

AC conductivity experiments as a function of frequency and temperature were developed for understanding the charge carrier transport mechanism in $(Bi_{0.5}Na_{0.5})_{0.935}Ba_{0.065}TiO_3$, (Figure 1). The AC conductivity shows a strong dependence on frequency in the range of frequencies studied. However, there was an increase in the conductivity at both high frequencies and temperatures, indicating that the conduction mechanism was thermally activated. In this type of material, the conduction mechanism is

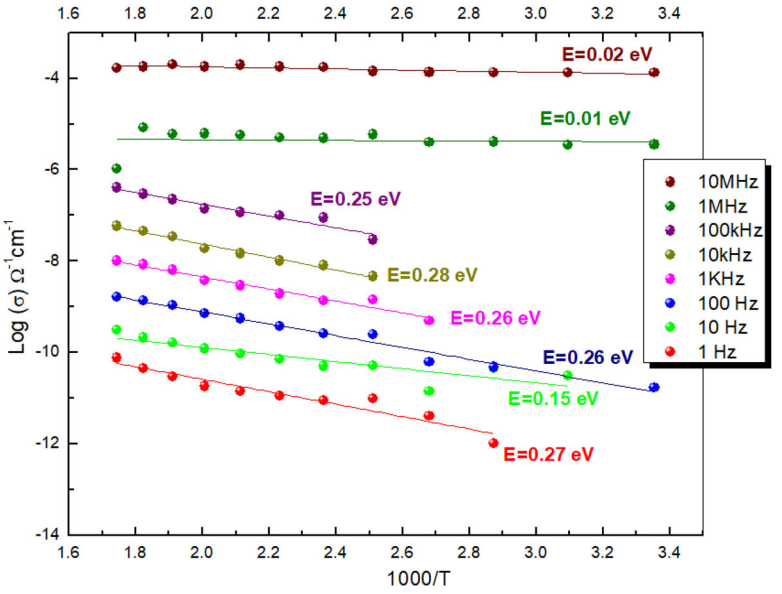

Figure 2. Arrhenius plot of the conductivity for poled BNBT (0.935/0.065).

associated with ionic conduction of the ions located at site A of the perovskite structure. Although conduction due to oxygen vacancies can be present due to the behavior of conductivity plot at frequencies higher than 100 KHz the results indicate that poled BNBT (0.935/0.065) follows the universal Jonscher law [46], suggesting short-range conductivity due to heterogeneous potential wells in this type of material.

Low-frequency dispersion (LFD) [47] was observed, which supports the idea of the presence of heterogeneous potential wells due to the presence of Na^{+}, Ba^{2+}, and Bi^{3+} cations in the structure. At frequencies higher than 1 MHz, the real component of conductivity overlaps at all the temperatures studied, suggesting that the conduction process at these frequencies was not thermally activated. The behavior at high frequencies was associated with a cooperatve effect between oxygen dipole fluctuations and electronic hopping [39, 48].

On the other hand, the conductivity decreases eight orders of magnitude from high frequency to low frequency, suggesting a blocking of the conduction pathways at low frequencies due to ion movement in A site of the perovskite structure.

The conductivity as a function of temperature was studied at specific frequencies ranging from 1 Hz to 10 MHz (Figure 2) in steps of one decade of frequency; conductivity serves to elucidate the existence of other effects on the electrical response. The results show high conductivity at 10 MHz, and conductivity also increases proportionally to the temperature. Mahto et al. [49] observed similar behavior for the $Ba_{0.06}Na_{0.47}Bi_{0.47}TiO_3$ type of material. There was an increase in the conductivity at high temperatures following the tendency presented in similar materials [28]. The obtained results point out that electron hopping is the primary conduction process at high frequency for this type of material. This contribution is also associated with the structural defects on poled BNBT, specifically oxygen vacancies created within the bulk due to the loss of

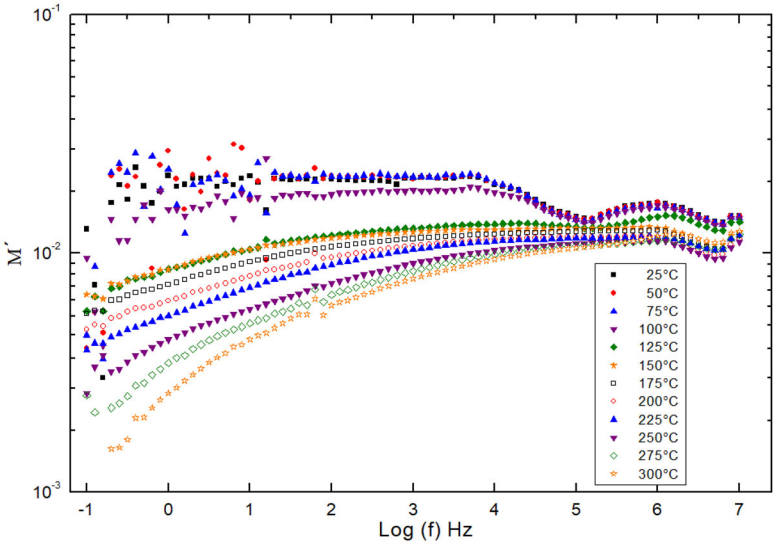

Figure 3. The real component of the electric modulus for poled BNBT (0.935/0.065).

oxygen during sintering. The literature reports that this process allows for charge compensation following the Kröger–Vink equation as follows [7, 48, 49]:

$$O_0 \rightarrow \frac{1}{2}\ O_2 \uparrow + V_0^{\cdot\cdot} + 2e^- \tag{1}$$

Therefore, some electrons overcame the potential well, hopping to neighboring sites at high frequencies (Figure 1).

The activation energy presented values in the range of 0.01–0.28 eV (Figure 2), below that reported for the acceptor-doped $Na_{0.5}Bi_{0.5}TiO_3$ perovskite [5], suggesting that control of the stoichiometry and the nature of the dopant cation are critical parameters when preparing this type of material in advanced technological applications. The activation energy remains the same until 100 kHz while, at highest frequencies decrease, suggesting that the mainly transport mechanism at low frequencies is ionic conduction, the electrical conduction mechanism was independent of the temperature at 1 MHz and 10 MHz [48, 50]. BNBT have been reported as ionic conductor [48, 50], and the obtained values of activation energy below 1 MHz agreed with this conduction mechanism. By the other hand, Yang et al. [5] suggested that its ionic conductivity comes from both Bi^{3+} ions (highly polarizable) and weak Bi–O bonds. However, considering the structural arrangement and the defects reported for this type of material, the results suggest a cooperative effect between free electrons and the oxygen dipole fluctuation favored by the vacancies created with the incorporation of Ba^{2+} ions in the unit cell.

The electrical modulus (Figure 3) was plotted to support the experimental evidence for electron hopping or short-range conductivity in poled BNBT (0.935/0.065). Electron hopping was evident due to the presence of the broad peak in the real component of the electrical modulus [28] around 1 MHz (Figure 3). Also, the plot indicated displacement of the modulus peak of one decade of frequency toward high frequencies.

The real component of the dielectric permittivity as a function of frequency and temperature was studied for elucidating additional contribution to the electrical

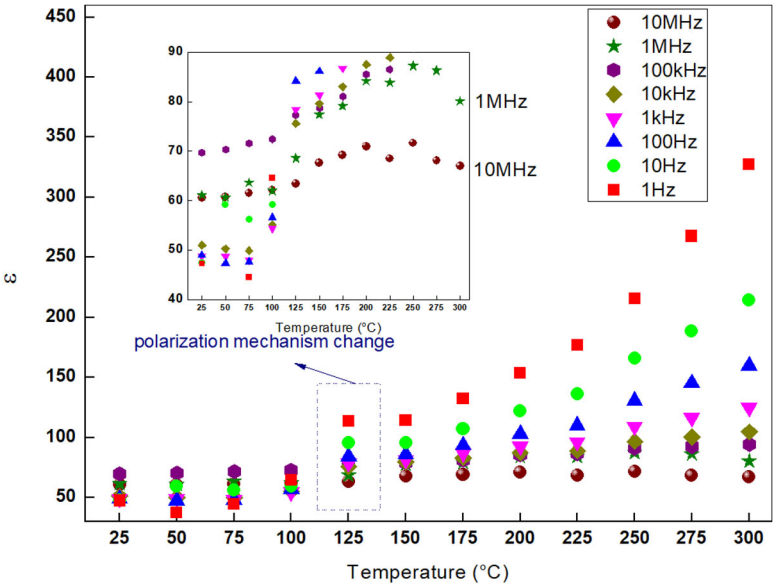

Figure 4. Dielectric permittivity comparison and temperature behavior for poled BNBT (0.935/0.065).

behavior (Figure 4), as a dipolar fluctuation in response to the electrical stimulus. The results show a step increase in the permittivity at 125 °C for all frequencies analyzed. This temperature is related to the ferroelectric to paraelectric transition that strongly depends on the dopant proportion [51–53]. The dielectric permittivity exhibited a broad peak around 200 °C and 250 °C at 10 MHz and 1 MHz frequency, respectively. An increment in the permittivity at lower frequencies and higher temperatures following an exponential tendency is also noted. At those frequencies, the reorientation of the electrical dipoles generated a delay in the relaxation time [54] due to the decrease in the ability of the dipole to return to the equilibrium position. This behavior is associated with the lattice disorder [55] induced by doping Ba^{2+} in the perovskite structure as it was discussed before. Also, the presence of Bi^{3+} in the A site of the perovskite structure modified the conduction pathways due to the Bi^{+3} ion having higher polarizability and a higher atomic mass than Na^{+} and Ba^{2+}. Thus, the dipole generated by the interaction between Bi and O in Bi–O created a delay in the relaxation time. The shortened dipole distance [56] provokes the reduction of the dielectric constant, promoting the appearance of the jump observed at 10 MHz and 1 MHz between 125 °C and 300 °C.

Tan δ versus frequency was studied to evaluate the energetic losses due to the interaction between the material and the electrical field (Figure 5). This plot shows a broad peak around 31 kHz for temperatures of 25–100 °C. At higher temperatures, there was a displacement on the inflection point. This displacement was associated with the variation of the loss energy mechanism induced by the dipole distortion as a response to the increase in atomic thermal vibrations at higher temperatures.

The tan δ versus temperature plot (Figure 6) shows a change around 125 °C. From this temperature to higher temperatures, tan δ shows an exponential behavior, consistent with the change in the mechanism of energy losses described above.

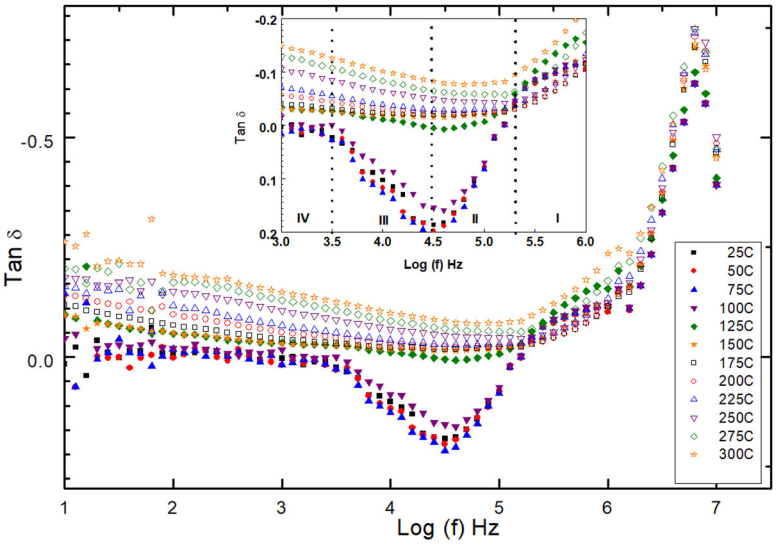

Figure 5. Loss tangent for poled BNBT (0.935/0.065).

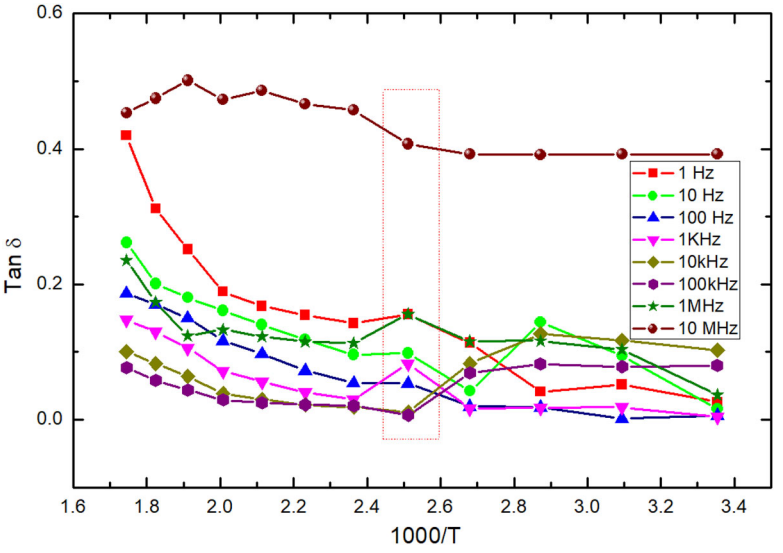

Figure 6. Tan δ vs. temperature for poled BNBT (0.935/0.065).

3.2. Structural characterization, rietveld refinement, and their relationship with the electrical behavior of $(Bi_{0.5}Na_{0.5})_{0.935}Ba_{0.065}TiO_3$

X-Ray diffraction experiments were performed for a better understanding of the structural effects of the electrical behavior of $(Bi_{0.5}Na_{0.5})_{0.935}Ba_{0.065}TiO_3$ (Figure 7). The X-ray pattern showed reflection peaks located at 22.61, 32.36, 40.10, 46.06, 46.54, 52.45, 57.58, 58.06, 67.50, 68.20, 72.34, 77.50, 81.06, 81.96, and 86.73° in 2θ with interplanar spacings of 3.93, 3.90, 2.76, 2.25, 1.97, 1.95, 1.74, 1.60, 1.59, 1.39, 1.37, 1.29, 1.25, 1.23, 1.18, 1.17, and 1.12 Å. These peak reflections are characteristic of the perovskite type of material reported in the literature.

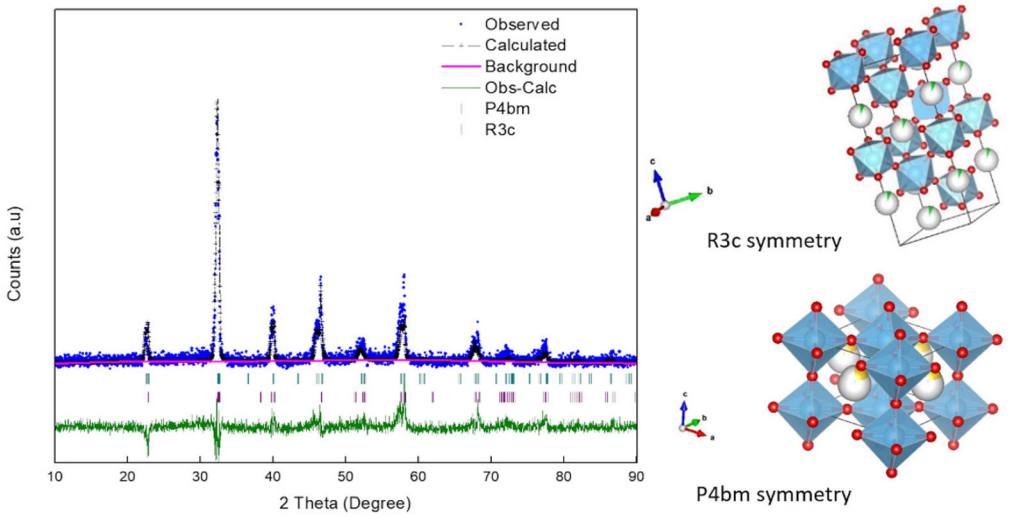

Figure 7. Rietveld refinement and polyhedral structures for poled $(Bi_{0.5}Na_{0.5})_{0.935}Ba_{0.065}TiO_3$. Red, O; blue, Ti; gray, Ba; yellow, Na; and green, Bi.

Rietveld refinement was performed to identify the crystal symmetry of the obtained poled $(Bi_{0.5}Na_{0.5})_{0.935}Ba_{0.065}TiO_3$. The starting structure was taken from an open crystallographic database with a card number of 2103296 (P4bm symmetry). The obtained goodness of fit (GOF) was 1.669. A second crystallographic phase was introduced in the refinement (card number 1532916, R3c symmetry) to improve the GOF. A summary of the Rietveld refinement results is shown in Table 1. The GOF was reduced to 1.555, and the theoretical XRD pattern was in good agreement with the experimental pattern (Figure 7). The Rietveld refinement indicated a mixture of two crystallographic phases, one with trigonal (R3c, Z6) symmetries and the other with tetragonal (P4bm, Z2) symmetries. The trigonal phase corresponds to 70 w% of the obtained material under the synthesis method applied in this work. The crystallographic planes found for the trigonal phase were $(10\bar{2})$, (104), (202), $(20\bar{4})$, (116), (214), (1010), and $(20\bar{1}0)$. For the tetragonal phase of poled $(Bi_{0.5}Na_{0.5})_{0.935}Ba_{0.065}TiO_3$, the following crystallographic planes were found: (001), (111), (201), (002), (202), (222), (400), (113), (331), (203), and (402). The polyhedral plot for both symmetries is shown in Figure 7, and the atomic position can be observed in Table 1.

Brian Toby [57], discuss R factors in Rietveld refinement and indicates that these indices measure the goodness of the background fitting, diffraction positions, and peak shapes, not just how well the structural model fits the diffraction intensities. Taken it into account, the results for R factor showed in Table 1, indicates proper fitting of the background, diffraction positions, and peak shapes.

3.2.1. Structure-electrical behavior ratio

From a structural point of view, the presence of the trigonal phase of poled $(Bi_{0.5}Na_{0.5})_{0.935}Ba_{0.065}TiO_3$ can explain the paraelectric-ferroelectric behavior between 125 °C and 300 °C at 1 MHz and 10 MHz (Figure 4). The Rietveld refinement indicated 46 atoms per unit cell in trigonal poled $(Bi_{0.5}Na_{0.5})_{0.935}Ba_{0.065}TiO_3$. Meanwhile, this was

Table 1. Rietveld refinement results.

Space group		R3c	P4bm
Occupancy factor	Bi	0.468	0.468
	Na	0.468	0.468
	Ba	0.065	0.065
	Ti	1	1
	O1	1	1
	O2	N.A	1
Crystallographic parameters	a = b	5.491378	5.895667
	c	13.586667	3.933674
	Volume (Å^3)	118.8062	354.8185
	Crystallographic density (g/cm^3)	5.9922	5.9653
	Perpendicular crystal size	213	145
	Parallel crystal size	183	298
	Mass	1280.312	426.771
	Z	6	2
	Scaling factor Weight %	0.37651 70	4.4261 30
Final agreement factors	χ^2 (chi^2)	1.555	
	R_p	25.3%	
	R_{wp}	32.8%	
	R_f	38.4 %	
	R_{exp}	24.7%	
Bond distance (Å)	Ti–O1	1.933	1.889
	Ti–O2	1.974	2.044
	Bi–O	2.603	2.509
	Ba–O	2.603	2.529
	Na–O	2.604	2.334

10 for the tetragonal cell. Hence, considering that the trigonal symmetry has the highest atom density per unit cell (Table 1) of both symmetries found in this material, the interaction between the electron clouds in the trigonal unit cell delays the orientation of dipoles, causing the decrease in the permittivity below 125 °C. The trigonal phase probably changed to the tetragonal phase after 125 °C, modifying the permittivity response at low frequencies.

The aspect ratio (parallel crystal size/perpendicular crystal size) was higher for the trigonal poled BNBT (0.935/0.065) (1.2) than the tetragonal poled BNBT (0.935/0.065) (0.5). Consequently, the anisotropy on the crystal size modified the dielectric response for both structures (Table 1). The shorter bound length of Ti–O in the tetragonal symmetry (Table 1) affects the electrical permittivity at temperatures higher than 125 °C (Figure 4) and the ionic conductivity in this structure (Figure 1); therefore, we can find an increase in the real component of the permittivity, as seen in Figure 4.

4. Conclusion

Poled $(Bi_{0.5}Na_{0.5})_{0.935}Ba_{0.065}TiO_3$ was successfully synthesized, and the ceramic material showed a low-frequency dispersion associated with the presence of Ba^{2+}, Bi^{3+}, and Na^{+} in the A site of this perovskite type of structure. Also, it was found electron hopping mechanism and oxygen dipole fluctuation as mainly transport mechanism in this material. There was evidence of a phase change at 125° C. The paraelectric-ferroelectric behavior was associated with the mixture of R3c (70%) and P4bm (30%) space groups.

Acknowledgments

The authors thank Vicerrectoría de Investigacion, Ciencia y Tecnología, Universidad de Boyaca, and Dirección de Investigación (DIMA) of Universidad Nacional de Colombia Sede Manizales for the financial support.

References

[1] K. Uchino, *Ferroelectric Devices* (Marcel Dekker, Boca Raton, FL, 2000).
[2] P. K. Panda, Review: environmental friendly lead-free piezoelectric materials, *J. Mater. Sci.* **44** (19), 5049 (2009). DOI: 10.1007/s10853-009-3643-0.
[3] P. K. Panda and B. Sahoo, PZT to lead free piezo ceramics: a review, *Ferroelectrics* **474** (1), 128 (2015). DOI: 10.1080/00150193.2015.997146.
[4] M. Li *et al.*, A family of oxide ion conductors based on the ferroelectric perovskite $Na_{0.5}Bi_{0.5}TiO_3$, *Nat. Mater.* **13** (1), 31 (2014).
[5] F. Yang *et al.*, Optimisation of oxide-ion conductivity in acceptor-doped $Na_{0.5}Bi_{0.5}TiO_3$ perovskite: approaching the limit? *J. Mater. Chem. A* **5** (41), 21658 (2017). DOI: 10.1039/C7TA07667C.
[6] Y. Lu *et al.*, Insight into the structure and functional application of Mg-doped $Na_{0.5}Bi_{0.5}TiO_3$ electrolyte for solid oxide fuel cells, *J. Alloys Compd.* **752**, 213 (2018). DOI: 10.1016/j.jallcom.2018.04.037.
[7] W. G. Wang and. X. Y. Li, Impedance and dielectric relaxation spectroscopy studies on the calcium modified $Na_{0.5}Bi_{0.44}Ca_{0.06}TiO_{2.97}$ ceramics, *AIP Adv.* **7** (12), 125318 (2017). DOI: 10.1063/1.5012108.
[8] J. Suchanicz *et al.*, Influence of Sr addition on structural, dielectric and Raman properties of $Na_{0.5}Bi_{0.5}TiO_3$ ceramics, *Integr. Ferroelectr.* **173** (1), 59 (2016). DOI: 10.1080/10584587.2016.1184498.
[9] R. Kumari *et al.*, Phase transformation and impedance spectroscopic study of Ba substituted $Na_{0.5}Bi_{0.5}TiO_3$ ceramics, *J. Alloys Compd.* **676**, 452 (2016). DOI: 10.1016/j.jallcom.2016.03.088.
[10] C. Feng *et al.*, Substrate-dependent ferroelectric and dielectric properties of Mn doped $Na_{0.5}Bi_{0.5}TiO_3$ thin films derived by chemical solution decomposition, *J. Alloys Compd.* **679**, 133 (2016). DOI: 10.1016/j.jallcom.2016.04.045.
[11] H. T. Sui *et al.*, Dielectric tunability of highly (l00)-oriented Fe-doped $Na_{0.5}Bi_{0.5}TiO_3$ thin film, *Ceram. Int.* **40** (8), 12989 (2014). DOI: 10.1016/j.ceramint.2014.04.161.
[12] Y. Wang *et al.*, Room-temperature ferromagnetism of Co-doped $Na_{0.5}Bi_{0.5}TiO_3$: diluted magnetic ferroelectrics, *J. Alloys Compd.* **475** (1-2), L25 (2009). DOI: 10.1016/j.jallcom.2008.07.073.
[13] S. K. Pradhan and S. K. De, Dielectric and optical properties of Ni doped $Na_{0.5}Bi_{0.5}TiO_3$, *Ceram. Int.* **44** (13), 15181 (2018). DOI: 10.1016/j.ceramint.2018.05.158.
[14] J. Qian *et al.*, The crystallization and dielectric tunability of Zn doped $Na_{0.5}Bi_{0.5}TiO_3$ thin films, *Ceram. Int.* **42** (1), 976 (2016). DOI: 10.1016/j.ceramint.2015.08.110.
[15] C. H. Yang *et al.*, Enhanced ferroelectric and dielectric properties of Nb^{5+}-doped $Na_{0.5}Bi_{0.5}TiO_3$ thin film deposited under nitrogen annealing atmosphere, *Ceram. Int.* **41** (8), 10272 (2015). DOI: 10.1016/j.ceramint.2015.03.022.
[16] X. M. Jiang *et al.*, Effects of annealing temperature on the microstructure, ferroelectric and dielectric properties of W-doped $Na_{0.5}Bi_{0.5}TiO_3$ thin films, *Ceram. Int.* **42** (10), 12210 (2016). DOI: 10.1016/j.ceramint.2016.04.163.
[17] S. Supriya *et al.*, Analysis of single and binary phases in cerium doped sodium bismuth titanate $Na_{0,5}Bi_{(0,5-x)}CexTiO_3$, *Boletín de la Sociedad Española de Cerámica y Vidrio* **54** (6), 225 (2015). DOI: 10.1016/j.bsecv.2015.11.002.
[18] L. Ma *et al.*, Dielectric and piezoelectric properties of (Li, Ce) modified $NaBi_5Ti_5O_{18}$ composite ceramics, *J. Rare Earths* **27** (3), 496 (2009). DOI: 10.1016/S1002-0721(08)60276-8.

[19] A. Franco, P. Banerjee, and P. L. Romanholo, Effect of composition induced transition in the optical band-gap, dielectric and magnetic properties of Gd doped $Na_{0.5}Bi_{0.5}TiO_3$ complex perovskite, *J. Alloys Compd.* **764**, 122 (2018). DOI: 10.1016/j.jallcom.2018.06.007.

[20] M. Zannen *et al.*, Structural, optical, and electrical properties of Nd-doped $Na_{0.5}Bi_{0.5}TiO_3$, *Mater. Chem. Phys.* **134** (2-3), 829 (2012). DOI: 10.1016/j.matchemphys.2012.03.076.

[21] L. Jiang *et al.*, Bright up-conversion emission of Er^{3+}-doped lead-free ferroelectric $Na_{0.5}Bi_{0.5}TiO_3$ single crystal, *Mater. Lett.* **210**, 158 (2018). DOI: 10.1016/j.matlet.2017.08.135.

[22] V. H. Schmidt, N. Archer, and C.-S. Tu, Impedance spectroscopy of bismuth sodium titanate: barium titanate ceramics with manganese doping, *J. Am. Ceram. Soc.* **101** (2), 713 (2018). DOI: 10.1111/jace.15236.

[23] R.-y. Jing *et al.*, Comparative study on structure, dielectric, and piezoelectric properties of $(Na_{0.47}Bi_{0.47}Ba_{0.06})_{0.95}A_{0.05}TiO_3$ ($A = Ca^{2+}/Sr^{2+}$) ceramics: effect of radii of A-site cations, *J. Eur. Ceram. Soc.* **38** (9), 3111 (2018). DOI: 10.1016/j.jeurceramsoc.2018.03.011.

[24] J. d. J. A. Flores-Cuautle, A. Cruz-Orea, and E. Suaste-Gómez, UV response of $(Bi_{0.5}Na_{0.5})_{0.935}Ba_{0.065}TiO_3$ lead free piezoelectric ceramics, *Adv. Sci. Lett.* **19** (3), 1052 (2013). DOI: 10.1166/asl.2013.4868.

[25] J. J. A. Flores-Cuautle, A. Cruz-Orea, and E. S. GÓMez, Determination of thermal diffusivity and thermal effusivity of the $(Bi_{0.5}Na_{0.5})_{0.935}Ba_{0.065}TiO_3$ ferroelectric ceramics by photothermal techniques, *Ferroelectr. Lett. Sect.* **35** (5-6), 136 (2008). DOI: 10.1080/07315170802520144.

[26] Z. Chen and J. Hu, Piezoelectric and dielectric properties of $(Bi_{0.5}Na_{0.5})_{0.94}Ba_{0.06}TiO_3$–$Ba(Zr_{0.04}Ti_{0.96})O_3$ lead-free piezoelectric ceramics, *Ceram. Int.* **35** (1), 111 (2009). DOI: 10.1016/j.ceramint.2007.09.110.

[27] C. Wang *et al.*, Electric field-induced giant strain and piezoelectricity enhancement effect in $(Bi_{1/2}Na_{1/2})_{0.935+x}Ba_{0.065}Ti_{1-x(}Pr_{1/2}Nb_{1/2})xO_3$ lead-free ceramics, *Ceram. Int.* **42** (3), 4354 (2016). DOI: 10.1016/j.ceramint.2015.11.114.

[28] K. R. Ansu, P. Kamal, and P. Ashutosh, Piezoelectric, impedance, electric modulus and AC conductivity studies on $(Bi_{0.5}Na_{0.5})_{0.95}Ba_{0.05}TiO_3$ ceramic, *Process. Appl. Ceram.* **7** (2), 81 (2013).

[29] R. Amini *et al.*, Structural, microstructural and thermal properties of lead-free bismuth--sodium–barium–titanate piezoceramics synthesized by mechanical alloying, *Mater. Res. Bull.* **48** (2), 482 (2013). DOI: 10.1016/j.materresbull.2012.11.008.

[30] T. Chen *et al.*, Effect of HfO2 content on the microstructure and piezoelectric properties of $(Bi_{0.5}Na_{0.5})_{0.94}Ba_{0.06}TiO_3$ lead-free ceramics, *Ceram. Int.* **40** (2), 2959 (2014). DOI: 10.1016/j.ceramint.2013.10.013.

[31] X. Y. Zhou *et al.*, Piezoelectric properties of Mn-doped $(Na_{0.5}Bi_{0.5})_{0.92}Ba_{0.08}TiO_3$ ceramics, *Mater. Lett.* **59** (13), 1649 (2005). DOI: 10.1016/j.matlet.2005.01.034.

[32] R. RodrÍguez-Ruiz *et al.*, Determination of the pyroelectric coefficient for (Bi0.5Na0.5) 0.935Ba0.065TiO3 piezoelectric ceramics, *Ferroelectrics* **368** (1), 216 (2008). DOI: 10.1080/00150190802368537.

[33] R. RodrÍguez-Ruiz, R. González-Ballesteros, J. J. A. Flores Cuautle, and E. S. Suaste-Gómez, Determination of the pyroelectric coefficient of the $(Bi_{1/2}Na_{1/2})_{0.935}Ba_{0.065}TiO_3$, presented at the Book of abstracts of the European Meeting on Ferroelectricity, Bled, Slovenia 181, 3–7 September 2010.

[34] N. Zhao *et al.*, Dielectric, conductivity and piezoelectric properties in $(0.67\text{-}x)BiFeO_3$-$0.33BaTiO_{3\text{-}x}SrZrO_3$ ceramics, *Ceram. Int.* **44** (15), 18821 (2018). DOI: 10.1016/j.ceramint.2018.07.116.

[35] N. Zhao *et al.*, Temperature-stable dielectric and energy storage properties of $La(Ti_{0.5}Mg_{0.5})O_3$-doped $(Bi_{0.5}Na_{0.5})TiO_3$-$(Sr_{0.7}Bi_{0.2})TiO_3$ lead-free ceramics, *J. Am. Ceram. Soc.* **101** (12), 5578 (2018). DOI: 10.1111/jace.15870.

[36] Y. Guo *et al.*, Electromechanical and electrical properties of $Bi_{0.5}Na_{0.5}Ti_{1-x}MnxO_{3-\delta}$ ceramics with high remnant polarization, *J. Alloys Compd.* **610**, 189 (2014). DOI: 10.1016/j.jallcom.2014.04.038.

[37] S. Ke *et al.*, Dielectric dispersion behavior of $Ba(ZrxTi_{1-x})O_3$ solid solutions with a quasi-ferroelectric state, *J. Appl. Phys.* **104** (3), 034108 (2008). DOI: 10.1063/1.2964088.

[38] M. Zou *et al.*, Microstructure and electrical properties of $(1-x)[_{0.82}Bi_{0.5}Na_{0.5}TiO_{3-0.18}$ $Bi_{0.5}K_{0.5}TiO_3]$–$xBiFeO_3$ lead-free piezoelectric ceramics, *J. Alloys Compd.* **495** (1), 280 (2010). DOI: 10.1016/j.jallcom.2010.02.025.

[39] O. Giraldo, N. P. Arias, and M. E. Becerra, Electrical properties of TiO_2-pillared bidimensional manganese oxides, *Appl. Clay Sci.* **141**, 157 (2017). DOI: 10.1016/j.clay.2017.02.019.

[40] N. Sahu and S. Panigrahi, Rietveld analysis, dielectric and impedance behaviour of Mn3+/Fe^{3+} ion-modified $Pb(Zr_{0\cdot65}Ti_{0\cdot35})O_3$ perovskite, *Bull. Mater. Sci.* **36** (4), 699 (2013). DOI: 10.1007/s12034-013-0522-8.

[41] B. Behera, P. Nayak, and R. N. P. Choudhary, Structural and electrical properties of $LiBa_2V_5O_{15}$ ceramics, *Phys. Stat. Sol. A* **204** (7), 2479 (2007). DOI: 10.1002/pssa.200622592.

[42] L. B. McCusker *et al.*, Rietveld refinement guidelines, *J. Appl. Crystallogr.* **32** (1), 36 (1999). DOI: 10.1107/S0021889898009856.

[43] A. C. Larson and R. B. Von Dreele. General Structure Analysis System (GSAS) Los Alamos National Laboratory 2000 Report LAUR 86–748, 2000.

[44] B. Toby, EXPGUI, a graphical user interface for GSAS, *J. Appl. Crystallogr.* **34** (2), 210 (2001). DOI: 10.1107/S0021889801002242.

[45] K. Momma and F. Izumi, VESTA 3 for three-dimensional visualization of crystal, volumetric and morphology data, *J. Appl. Crystallogr.* **44** (6), 1272 (2011). DOI: 10.1107/S0021889811038970.

[46] A. K. Jonscher, Frequency-dependence of conductivity in hopping systems, *J. Non-Cryst. Solids* **8-10**, 293 (1972). DOI: 10.1016/0022-3093(72)90151-2.

[47] A. K. Jonscher, Admittance spectroscopy of systems showing low-frequency dispersion, *Electrochim. Acta* **35** (10), 1595 (1990). DOI: 10.1016/0013-4686(90)80015-G.

[48] F. Yang, P. Wu, and D. C. Sinclair, Enhanced bulk conductivity of A-site divalent acceptor-doped non-stoichiometric sodium bismuth titanate, *Solid State Ionics* **299**, 38 (2017). DOI: 10.1016/j.ssi.2016.09.016.

[49] U. K. Mahto, S. K. Roy, and K. Prasad, High energy milled $Ba_{0.06}Na_{0.47}Bi_{0.47}TiO_3$ceramic: structural and electrical properties, *IEEE Trans. Dielectr. Electr. Insul.* **25** (1), 174 (2018). DOI: 10.1109/TDEI.2018.006624.

[50] F. Yang *et al.*, High ionic conductivity with low degradation in A-site strontium-doped nonstoichiometric sodium bismuth titanate perovskite, *Chem. Mater.* **28** (15), 5269 (2016). DOI: 10.1021/acs.chemmater.6b02555.

[51] N. D. Scarisoreanu *et al.*, *Phase Transitions, Dielectric and Ferroelectric Properties of Lead-free NBT-BT Thin Films, Advances in Ferroelectrics* (IntechOpen, Aimé Peláiz Barranco, 2012). https://www.intechopen.com/books/advances-in-ferroelectrics/phase-transitions-dielectric-and-ferroelectric-properties-of-lead-free-ferroelectric-nbt-bt-thin-fil.

[52] Y. Qu, D. Shan, and J. Song, Effect of A-site substitution on crystal component and dielectric properties in $Bi_{0.5}Na_{0.5}TiO_3$ ceramics, *Mater. Sci. Eng. B* **121** (1-2), 148 (2005). DOI: 10.1016/j.mseb.2005.03.023.

[53] K. L. Y. Meera Rawat *et al.*, Structural, dielectric and conductivity properties of Ba2 + doped $(Bi_{0.5}Na_{0.5})TiO_3$ ceramic, *Adv. Mater. Lett.* **3** (4), 286 (2012). DOI: 10.5185/amlett.2012.2322.

[54] T. Sahu and B. Behera, Relaxation processes and conduction mechanism in bismuth ferrite lead titanate composites, *J. Phys. Chem. Solids* **113**, 186 (2018). DOI: 10.1016/j.jpcs.2017.10.021.

[55] C. Cui *et al.*, Structure, dielectric and relaxor properties in lead-free ST-NBT ceramics for high energy storage applications, *J. Alloys Compd.* **711**, 319 (2017). DOI: 10.1016/j.jallcom.2017.04.023.

[56] R. Ulrich *et al.*, Comparison of paraelectric and ferroelectric materials for applications as dielectrics in thin film integrated capacitors, *Int. J. Microcircuits Electron. Packag.* **23** (2), 172 (2000).

[57] B. H. Toby, R factors in Rietveld analysis: how good is good enough? *Powder Diffr.* **21** (1), 67 (2006). DOI: 10.1154/1.2179804.